Pore Size-Dependent Structure of Confined Water in Mesoporous Silica Films from Water Adsorption-Desorption using ATR-FTIR Spectroscopy

*Bettina Baumgartner[1], Jakob Hayden[1], Jérôme Loizillon[2], Sophia Steinbacher[1], David Grosso[2], Bernhard Lendl[1,]**

[1]Research Division of Environmental Analytics, Process Analytics and Sensors, Institute of Chemical Technologies and Analytics, Technische Universität Wien, Getreidemarkt 9, 1060 Vienna, Austria

[2]NOVA Team, Institut Matériaux Microélectronique et Nanosciences de Provence, (IM2NP) - UMR CNRS 7334, Aix-Marseille Université, Faculté des Sciences de Saint Jérôme, 13397 Cedex 20 Marseille, France

ABSTRACT The local structure of water on chemically and structurally different surfaces is subject of ongoing research. In particular, confined spaces as found in mesoporous silica have a pronounced effect on the interplay between adsorbate-adsorbate and adsorbate-surface interactions. Mid-infrared spectroscopy is ideally suited to quantitatively and qualitatively study such systems as the probed molecular vibrations are highly sensitive to intermolecular interactions. Here, the quantity and structure of water adsorbed from the gas phase into silica mesopores at different water vapor pressures was monitored using mid-infrared attenuated total reflection (ATR) spectroscopy. Germanium ATR crystals were coated with different mesoporous silica films prepared by evaporation induced self-assembly. Quantitative analysis of the water bending vibration at 1640 cm^{-1} at varying vapor pressure allowed for retrieving porosity and pore size distribution of the mesoporous films. The results were in excellent agreement with those obtained from ellipsometric porosimetry. In addition, different degrees of hydrogen bonding of water as reflected in the band position and shape of the stretching vibrations (3000 - 3750 cm^{-1}) were analyzed and attributed to high-density, unordered bulk and low-density, surface-induced ordered water. Thereby, the progression of surface-induced ordered water and bulk water as a function of water vapor pressure was studied for different pore sizes. Small pores with 5 nm diameter showed a number of two ordered monolayers, while for pores > 12 nm the number of ordered monolayers is significantly larger and agrees with the number observed on planar SiO_2 surfaces.

INTRODUCTION

All applications of mesoporous materials in industry and research, such as (photo) catalysis,[1–3] separation,[4] electrochemistry,[5] or (bio-)sensing[6,7] benefit from the materials high-surface area and defined porosity. Their functionality and applicability in these various disciplines depends, however, not only on their large specific surface area, but fundamentally on the adsorbate-surface interactions. The latter play a pivotal role and drive researchers to investigate the bonding mechanisms *e.g.* H-bonding or π-π interactions. Such information is of particular interest for water at surfaces.[8,9] The understanding of the local structure of water, especially in confined spaces like mesopores, is still object of intensive studies.[10,11] Because of its high polarity, water and its manner of adsorption are strongly influenced by the surface's hydrophobicity and the H-bonding formed with the surface.[8,9,10,11] Infrared (IR) spectroscopy has proven an ideal method for studying adsorbed water, both qualitatively and quantitatively, as it is very sensitive to water and its states of hydrogen bonding.[9,12,13,14,15] The ν(O-H) stretching bands located between 3000 cm^{-1} and 3800 cm^{-1} give rich qualitative information as they are strongly affected by the molecule's environment and the structure of water. Several water complexes have been reported that can be distinguished within this region based on IR spectroscopy.[16,17] The second intense band of water, located at 1640 cm^{-1}, is attributed to the H-O-H bending and is widely insensitive to the molecular surrounding. Therefore, it can be used as a robust measure for the quantity of adsorbed water.

Although the plentiful information obtained from IR spectroscopy of water in mesoporous silica has been studied, *e.g.* for low temperatures and/or under static conditions,[16,17] the progression of water's local structure during adsorption/desorption has not been investigated yet. Measurements during adsorption/desorption from the gas phase at controlled humidity are hence needed to study the effect of the degree of pore filling on water's local structure. While such measurements have been reported for planar, dense SiO_2 films, the strong effects of confined spaces on the structure of adsorbed water sparks interest in a corresponding study on mesoporous materials that is yet pending.[15,18–20] In order to discuss the water adsorption/desorption process quantitatively and qualitatively, characteristic parameters such as porosity and pore size distribution (PSD) are needed. The well-characterized optical setup presented herein allows, for the first time, to use ATR spectroscopy for porosimetry. Using absolute water contents derived from IR spectra and a modified Kelvin equation, PSD and porosity can be calculated.

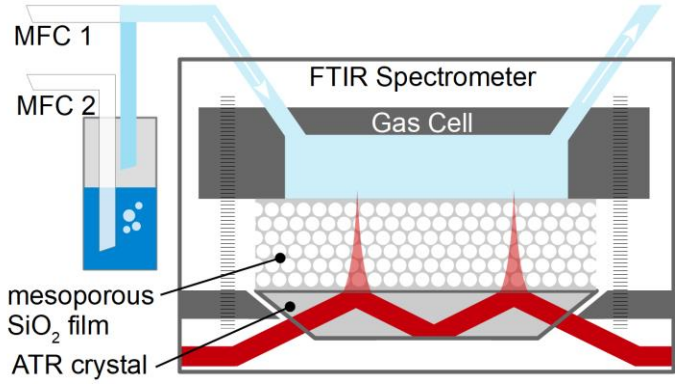

Scheme 1: Mesoporous silica film coated on ATR crystal (Germanium, 20 active bounces) placed in a flow cell that is inserted into the beam path of an FTIR spectrometer and purged with humidified air.

In this contribution, we present a method for determining porosity and PSD of mesoporous films using ATR FTIR spectroscopy non-destructively and at ambient conditions. Ge ATR crystals coated with mesoporous silica films of different pore size and arrangement were subjected to controlled humidity while monitoring the amount of adsorbed water per film volume (compare Scheme 1). Subsequently, PSD and porosity are retrieved from obtained isotherms using a modified Kelvin equation. The results were validated against ellipsometric porosimetry (EP),[21,22] a technique that has proven to be a particularly simple alternative to surface acoustic wave devices[23] and quartz micro balances[24]. Furthermore, we analyze the O-H stretching bands (symmetric and asymmetric) between 3800 cm^{-1} and 3000 cm^{-1} to derive information about the structure of adsorbed water and its progression during water adsorption/desorption. The spectra were deconvolved using six bands associated with differently coordinated water.[12,16] These bands can be categorized into vibrational modes corresponding to low-density (LD) and high-density (HD) water. We find that LD water accounts for the major fraction prior to pore condensation, while HD water constitutes the main fraction after pore condensation. Analyzing the area of the O-H stretching bands for varying humidity allows, for the first time, *in situ* monitoring of the humidity-dependent structure of adsorbed water in confined mesopores of silica films. Finally, we calculate the number of surface-induced ordered monolayers of water for two different pore sizes and demonstrate that the number is similar to planar SiO_2 surfaces only for big pores, while for smaller pores the number is significantly reduced.

EXPERIMENTAL DETAILS

Materials and Methods

Tetraethoxysilane (TEOS, Sigma Aldrich 99.5%), abs. ethanol (Fisher, 99.6%), hydrochloric acid (VWR, 37%), cetyltrimethylammonium bromide (CTAB, Sigma Aldrich, 99%), Pluronic F127 (Sigma Aldrich), were used as received.

The mesoporous silica thin films CTAB 3D hexagonal and CTAB cubic were synthesized as previously reported,[25] using evaporation induced self-assambly.[26] Shortly, sol compositions with final molar ratio of 1:13:5:0.005:0.12–0.16 for TEOS:EtOH:H_2O:HCl:CTAB with 0.12 eq CTAB for the 3D hexagonal and 0.16 eq CTAB for the cubic film, respectively, were heated at 40 °C for 4 h. The F127 film was prepared by stirring of ethanol, TEOS, water and 0.1 M HCl (molar ratio TEOS:ETOH:H_2O:HCl = 1:8.7:10.3:0.01) at room temperature for 20 min, followed by addition of a polymer solution to the sol. The resulting solution had a final molar ratio of TEOS:EtOH:F127:H_2O:HCl = 1:16:0.01:16.3:0.015 and the mixture was stirred for 3 h at room temperature. All three films were spin coated with a spinner velocity of 2000 rpm and subsequently

calcined at 400 °C for 12 h with a heating ramp of 1 K min^{-1}. Details on the characterization of mesoporous silica films are given in the ESI.

ATR FTIR Spectroscopy and Gas Handling

Mesoporous coatings were prepared on ATR crystals cut from double-side polished Germanium wafers into 20 x 10 x 0.5 mm pieces and the facets were polished to a defined angle of 45°. Note that double-side polished Si or Ge wafers can be used directly as ATR crystals without using angled facets. However, angled facets provide higher depths of penetration and larger optical throughput, yielding measurements of better signal to noise ratio.[27] This configuration allowed for 20 active reflections. These ATR crystals were placed in the beam path of a Bruker Vertex 80v spectrometer equipped with a liquid nitrogen cooled mercury–cadmium–telluride (MCT) detector (InfraRed Associates), as previously reported,[25] using a home-built aluminum gas cell with a volume of 4 cm^3. IR spectra were acquired with a spectral resolution of 4 cm^{-1} and a total of 32 scans (4 s, double-sided, backward forward acquisition mode) were averaged per spectrum. The noise level was evaluated as the RMS noise of 100% lines, which were obtained by calculating the absorbance spectrum of two subsequent single-beam spectra of the same sample under identical conditions. The RMS noise between 2000 and 1400 cm^{-1} was determined to be 4×10^{-5} A.U. from 32 averaged scans.

The controlled relative water vapor pressures were generated by mixing a dry N_2 flow with a moistened N_2 flow obtained from bubbling a metered flux through water at 50 °C by means of mass flow controllers (controlled using LabVIEW®,National Instruments). The total flux was fixed to 2 L min^{-1}. All vessels and the flow cell were connected by 6 mm O.D. tubing. The actual water relative vapor pressure was determined by transmission IR Spectroscopy in a 4 cm transmission cell with ZnSe windows. The observed ro-vibrational lines between 1800 – 1600 cm^{-1} were integrated and using a 1 ppm/m water spectrum obtained from the PNNL database the relative humidity present in the gas flux was calculated.

For all experiments, films were analyzed directly after calcination to avoid contamination from ambient environment. In addition, prior to every water adsorption/desorption measurement, the freshly calcined films were exposed to high humidity to rehydrate and stabilize the silanol groups on the surface.[21]

Ellipsometric Porosimetry

All films were analyzed by spectroscopic ellipsometry with a UV-visible variable angle spectroscopic ellipsometer (M2000, J.A. Woolam) equipped with a controlled atmospheric cell. Refractive index dispersions and film thicknesses were extracted from conventional Ψ and Δ fitting (where Ψ and Δ are the ratio of the amplitude diminutions and the phase difference induced by the reflection) using a Cauchy model (CompleteEASE software, J.A. Woolam) and measured under dry atmosphere. The porosities were calculated from the refractive index of the coatings using Bruggeman effective medium approximation. Water isotherms were obtained from EP

investigations performed on the films just after desorption at 200°C for 30 min to remove adsorbed VOCs. The H_2O relative vapor pressure was adjusted using mass flow controller systems (ACEflow, Solgelway). The flux was set at 5 L min^{-1}.

RESULTS AND DISCUSSION

Monitoring Water Adsorption and Desorption

Before every adsorption/desorption experiment the silica films were exposed to a dry airflow to remove water adsorbed from ambient air until the spectra were stable, which was typically achieved after 5 min. Afterwards, relative vapor pressures between p/p_0 = 0 – 0.95 and back to 0 with 2 min holding time at each step were applied to the silica films while recording spectra every 20 s. The thereby obtained spectra of adsorbed water into the mesoporous silica films as function of relative vapor pressure are given in Figure 1A. Bands associated with water are found in two spectral regions: The H-O-H bending vibration at 1640 cm^{-1}, and a group of bands between 3000 – 3800 cm^{-1} corresponding to symmetric and asymmetric O-H stretching vibrations. While the latter is greatly affected by water local structure and hydrogen bonding to itself and the surface (compare section "water film structure"), the bending vibration does not vary significantly. Therefore, its band height is used in this study as a robust quantitative measure for the amount of water adsorbed in the film.

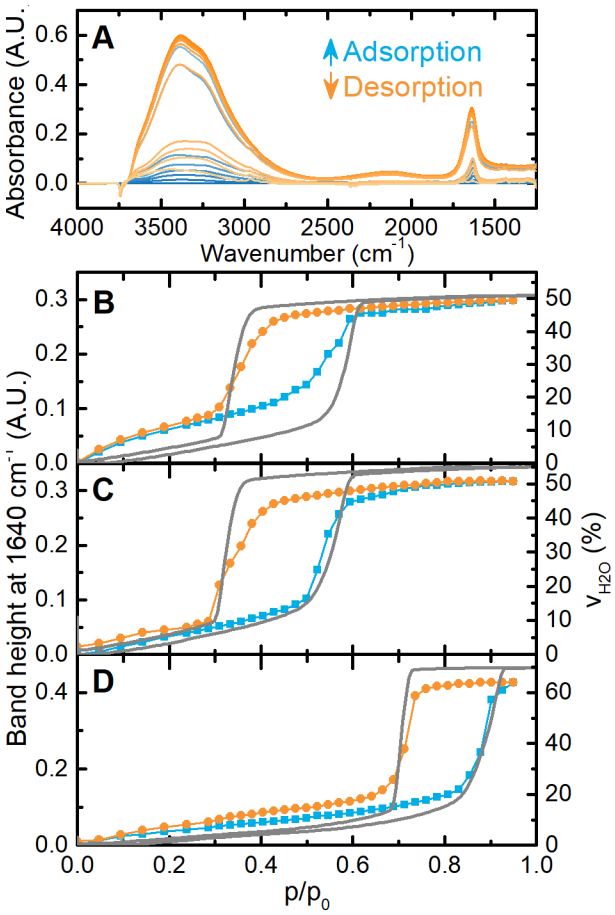

Figure 1: (A) Evolution of water spectra with adsorption (blue) and desorption (orange) of water vapor. Relative humidity is stepped by p/p_0=0.1 between consecutive spectra. Background taken at p/p_0=0. (B-D) Isotherms of CTAB 3D hexagonal film (B), CTAB cubic film (C), and F127 film obtained from IR experiments compared with ellipsometric porosimetry (gray).

For all films we find reversible isotherms type IV, according to IUPAC classification,[28] with the characteristic steep increase of water content upon capillary condensation in the mesopores and a hysteresis between adsorption and desorption branches. [28] The hysteresis can have different origins: (i) Change of meniscus between adsorption and desorption from cylindrical to spherical due to the formation of nucleation barriers (typically found in cylindrical pores);[29] or (ii) Pore blocking effects, which are due to the presence of interconnections of smaller size than the pores; *i.e.* bottleneck pores (small necks or mesopores connected through the intrinsic microporosity of the thin film). In this case, desorption can occur via the cavitation mechanism, leading to a very steep desorption step at $p/p_0 \approx 0.3$.

Retrieval of Adsorbed Water Concentration and Porosity

Calculating the porosity and PSD of the film requires calculating the volume fraction of adsorbed water per film unit volume, $v_{H2O} := V_{H2O}/V_{film}$, from the recorded values of absorption. To this end, we modified the theory for ATR spectroscopy at mesoporous films introduced previously.[25] The theory builds on Lambert-Beer's law

$$A = \varepsilon \cdot c \cdot d_{e,film} \cdot N \qquad \text{Equation 1}$$

Herein, $\varepsilon_{H2O,1640\ cm\text{-}1}$ = 21.4 L mol^{-1} cm^{-1} is the specific absorption coefficient of water, c is water's concentration in the film (given as n_{H2O} per V_{film}) and N the number of active bounces of the ATR element. $d_{e,film}$ is the effective pathlength within the film, defined as the effective pathlength commonly used in ATR spectroscopy,[30] scaled by the fraction of the evanescent field within the film (compare Scheme 1).[25] The initial $d_{e,film,0}$ is calculated assuming $n_{film} = n_{SiO2}$ =1.26 at 1640 cm^{-1}.[31] As the refractive index changes as a function of pore filling, this n_{film} is corrected by an iterative process yielding $d_{e,film,corr}$ (see below and ESI). Based on Equation 1, v_{H2O} can be calculated as the ratio of measured water absorbance in the silica film, $A_{H2O\ in\ film,}$ and the absorbance one would measure if no water was displaced by the silica network, *i.e.* if no silica film was on the ATR crystal but a water film with the same thickness (see Equation 2).

$$v_{H2O} = \frac{A_{H2O\ in\ SiO2\ film}}{A_{\ pure\ H2O}} = \frac{A_{H2O\ in\ SiO2\ film}}{\varepsilon_{H2O,1640cm-1} \cdot c_{pure\ H2O} \cdot d_{e,film,corr} \cdot N} \qquad \text{Equation 2}$$

Herein, $c_{pure\ H2O}$ = 55.6 mol L^{-1}. Equation 2 is valid if the absorption coefficient of adsorbed water is the same as for liquid water, which implies that water's density ρ = 1 g cm^{-3} does not change. Although previous studies found smaller water densities in mesoporous materials (ca. 0.9 g cm^{-3}),[32,33] we do not account for this, because data on the change of water density in the course of pore filling (compare section "Structure of Confined Water during Adsorption") as well as for different pore size is not available.

Table 1: Summary of calculated parameters, see ESI for calculations.

	$d_{e,film,0}\cdot N$ initial estimation	*Corrected* $d_{e,film,corr}\cdot N$ [µm] $p/p_0 = 0$	*Corrected* $d_{e,film,corr}\cdot N$ [µm] $p/p_0 = 0.95$	c_{H2O} [mol_{H2O}/dm^3_{film}] at $p/p_0 = 0.95$	Corrected Porosity (%)	Porosity from EP (%)	$n_{porous\ SiO2}$ at $p/p_0 = 0$; λ=6.1 µm
CTAB 3D hex	4.99	4.31	5.31	27.2	49	51	1.13
CTAB cubic	5.07	4.42	5.07	28.1	51	55	1.13
F127	5.44	4.51	5.68	35.4	63	68	1.09

[a]obtained from ratio of water concentration in film to complete water film with same thickness

The porosity *P* of the film is defined as the water fraction at fully filled pores at highest humidity, P:= $v_{H2O}(p/p_0$=0.95). As $d_{e,film}$ and hence v_{H2O} depends, amongst others, on the refractive index of the film, it changes significantly during adsorption experiments due to the displacement of air (n_{air}=1) by water (n_{H2O}=1.33). To take this into account in the calculation of *P*, we employ an iterative calculation (see ESI). The obtained corrected values of $d_{e,film}$ for p/p_0=0 and p/p_0=0.95 are given in Table 1 (see ESI for full range).

The films were furthermore characterized by EP and the hereby-obtained values for the porosity are as well given in Table 1. The corresponding isotherms are given in Figure 1B-D, showing good agreement with the values obtained by ATR spectroscopy. We attribute the small differences between calculated porosities (*i.e.* the height of the isotherms) to the wrong assumption for the density of water. In contrast to the density of 1 g cm^{-3} used herein, values of ca. 0.9 g cm^{-3} were reported and explained with either incomplete pore filling[32] or, as discussed later, the different nature of water in confined pores. Remaining differences between results obtained via ATR spectroscopy and EP may originate from small differences in the measurement setups as for EP the p/p_0 was ramped, while IR measurements were performed with a stepwise increase. Further discussion of the differences would require side-by-side measurements in the same laboratory under same conditions.

Pore Size Distribution

Similar to other porosimetry techniques, the isotherms obtained in the previous section were analyzed by the Kelvin equation to derive the pore size distribution.[21,34,22,35] The Kelvin equation describes the behavior of a fluid in confined spaces such as a capillary. The Kelvin radius r_K equals the radius of curvature of the meniscus formed in this capillary, which depends on the relative

vapor pressure p/p_0, surface tension γ, molar volume of the adsorbate V_m, contact angle θ, a geometric factor G, temperature T and gas constant R:

$$r_K = \frac{-G \cdot \gamma \cdot V_m \cdot \cos(\theta)}{R \cdot T \cdot \ln(\frac{P}{P_0})} \qquad \text{Equation 3}$$

$$\gamma = \gamma_0 (\frac{1}{1+\frac{G\delta}{r_K}}) \qquad \text{Equation 4}$$

The surface tension γ is a function of curvature and was modified by the Tolman model with a fixed Tolman length δ, with δ being the molecular diameter of adsorbate.[36,37] For the adsorbate water, γ_0=7.28·10^{-2} J m^{-2}, V_m = 18.04·10^{-6} m^3 mol^{-1}, θ=27° (obtained from contact angle measurements), R= 8.314 kg m^2 s^{-2} mol^{-1} K^{-1}, T=298 K, δ=9.6 10^{-11} m were inserted. The geometric factor G was calculated according to the Isotropic Inorganic Pore Contraction (IIC) model,[21] which describes the pore anisotropy resulting from the shrinkage of the film upon calcination (see ESI).

r_K solely describes the radius of curvature of the meniscus and for determining the actual pore diameter the thickness t of the adsorbate layer on the pore wall has to be added: $D_{pore} = 2(r_k + t)$.[38] As for gas sorption measurements, data on t is not available and needs to be estimated.[28] Due to the lack of data for porous materials, we use the film thickness t of water adsorbed on planar SiO_2 as a function of relative humidity as obtained from literature and fitted with a third order polynomial function (see ESI).[39,18] Finally, the pore size distribution is obtained following the BJH method,[40] by taking the derivative of the adsorbed volume v_{H2O} with respect to D_{pore} and plotting the result versus D_{pore} on the x-axis (see Figure 2). The hysteresis present in the isotherms is relatively large for water, characteristic of bottleneck pores as discussed in the previous section. In this case, the adsorption branch can be used to estimate the pore size whereas the desorption branch is associated to the interconnection size and not the pore size itself.[38,41] For both CTAB films desorption occurs at $p/p_0 \approx 0.3$, the typical experimentally obtained cavitation pressure for water in mesopores. This suggests that water desorbs under cavitation conditions rather than equilibrium conditions from these films as a similar behavior was reported for inert gases.[42,43] Thus, the interconnection size distributions may be overestimated. In contrast, the desorption branch obtained from the F127 film occurs at $p/p_0 > 0.3$ ($p/p_0 \approx 0.7$), therefore equilibrium desorption can be concluded and the obtained PSD reflects the real size distribution of the interconnections.

The obtained PSDs for all films were compared with the established EP. The results are included in Figure 2 and show excellent agreement with the PSDs obtained from ATR spectroscopy.

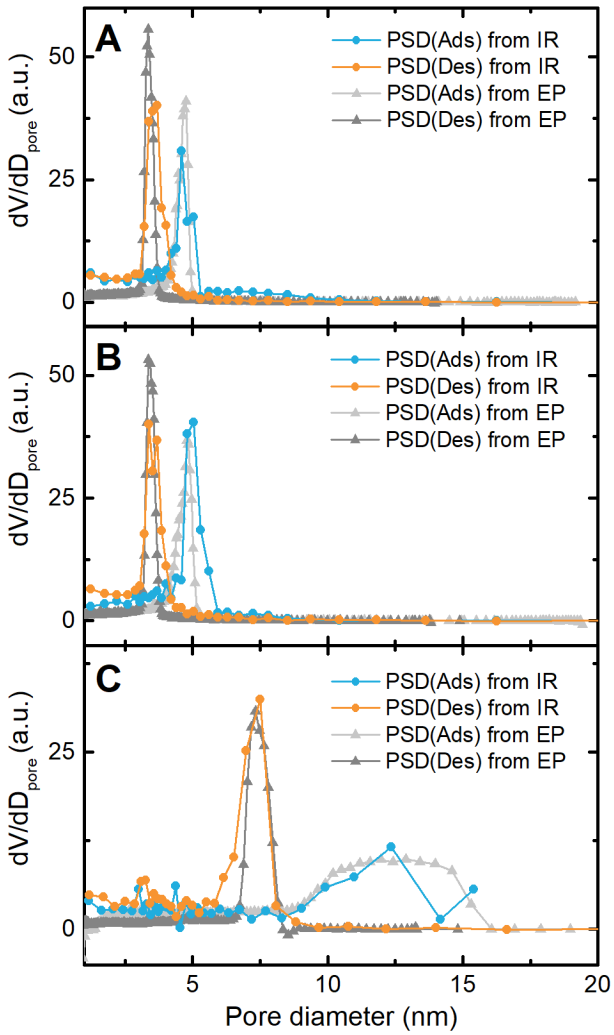

Figure 2: Pore Size Distribution of CTAB 3D hexagonal film (A), CTAB cubic film (B) and F127 film (C) obtained from ATR spectroscopy compared with the results of EP (gray).

Structure of Confined Water during Adsorption

O-H stretching vibrations and the less intense overtone of water's bending vibration between 3000 and 3800 cm^{-1} provide rich information about the structure of silica as well as the adsorbed water[44,45] Figure 3 shows a close-up of the normalized bands in this spectral region corresponding to the adsorption branch in Figure 1B.

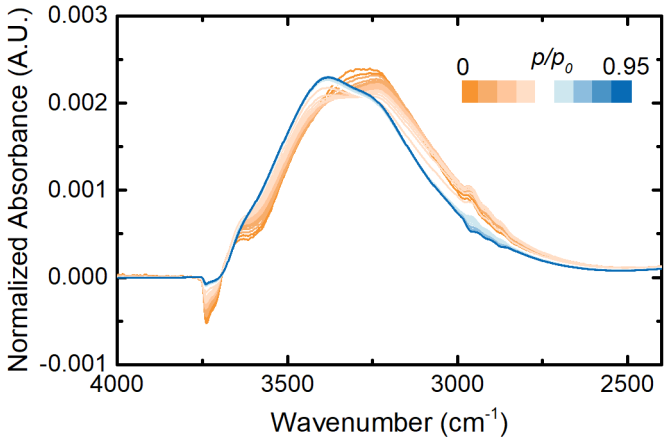

Figure 3: FTIR spectra of water adsorption into the 3D hexagonal film in the ν(O-H) region normalized to the entire band area between 2400 and 3800 cm^{-1}. Background spectrum was taken under dry ($p/p_0=0$) conditions. Bands between 3000 – 2800 cm^{-1} are attributed to hydrocarbons accumulated from the gas phase.

With increased filling of the pores, a clear shift in the maximum of the spectra from 3230 cm^{-1} to 3400 cm^{-1} is visible. This shift has been previously observed for planar silica surfaces and was attributed to different ratios of referred to as "ice-like" water (3230 cm^{-1}) and "liquid-like" water (3400 cm^{-1}) on SiO_2 films upon increasing relative humidity.[18] Asay *et al.* ascribe the "ice-like" character of the first monolayers of the adsorbed water to surface-induced ordering due to strong hydrogen bonding with the silica surface. After the third monolayer of water, this structuring effect decreases and the water band shifts to higher wavenumbers. Furthermore, Mallamace *et al.* studied water confined in mesoporous silica at low temperature using FTIR spectroscopy. They distinguished five bands within the ν(O-H) region: I) 3220 cm^{-1} attributed to fully bonded water of low density having a coordination number close to four, as observed in ice; II) 3400 cm^{-1} for water having an average degree of connection greater than for dimers and trimers but lower than for I), III) 3540 cm^{-1} corresponding to water molecules that are poorly connected to their environment, IV) 3620 cm^{-1} for water in trimers and tetramers, and V) 3140 cm^{-1} for a second local structure of low-density water.[16] Probing the local H-bonding environment of the water molecule via the band positions allows for correlating these bands with water's density.[12,16,46,47] The bands observed at higher frequencies (II-IV) were attributed to high-density (HD) water, whose local tetrahedrally coordinated H-bonding structures is not fully developed.[16] Here, water molecules exist in small clusters of up to four molecules. Bands I+V were attributed to low density water (LD water, with a density close to the one of ice).[12,16,46]

In the present study, an additional band at 3745 cm^{-1} was observed that corresponds to isolated silanol groups ν(Si-O-H) that exist only in anhydrous conditions. Due to their hydrophilic nature, these silanol groups are hydrated immediately if water vapor is present and since the background spectra are recorded on dry films this leads to the negative peak observed in Figure 3.[44] Since the silanol groups influence the hydrophilicity and hence the hydration mechanism of silica, the silanol

content was calculated for the CTAB 3D hexagonal and the F127 film (see ESI for details). Due to the similar Si-OH coverage for both films we assume similar wetting properties allowing a comparison of the two films.

The ν(O-H) region of the spectra obtained for the smallest (CTAB 3D hexagonal) and the biggest (F127) pore system were deconvolved, in accordance with Refs. [12,16], by fitting the spectra using six Gaussian profiles with fixed peak positions (3140, 3220, 3400, 3540, 3620 and 3745 cm^{-1}) and widths.[12,16] Here, the band fitting was adopted where different spectral bands were curve assigned to single absorption bands, where contributions of the asymmetric and symmetric stretch were combined into a single band. The results are given in Figure 4 and Figure 5, respectively.

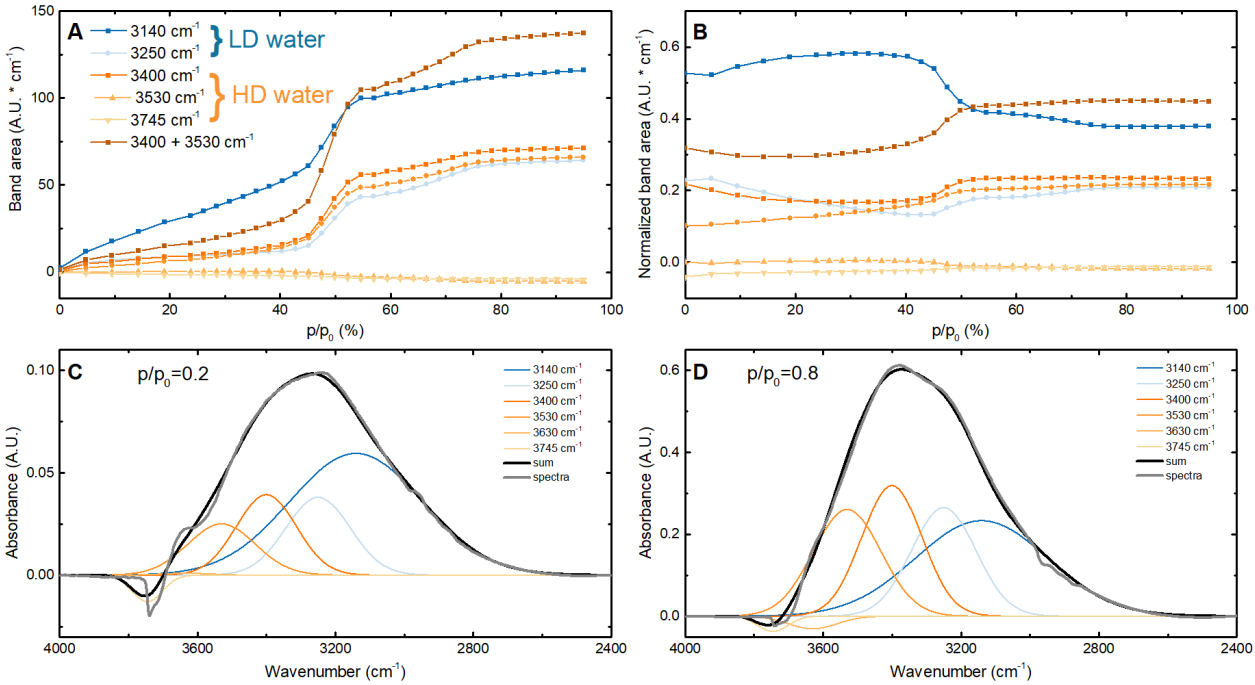

Figure 4: Deconvolution of ν(O-H) region obtained for CTAB 3D hexagonal film during increasing p/p_0: peak area for different bands (A), band area normalized to the total band areas (B), multi-Gaussian fit of spectra before (C) and after (D) pore condensation.

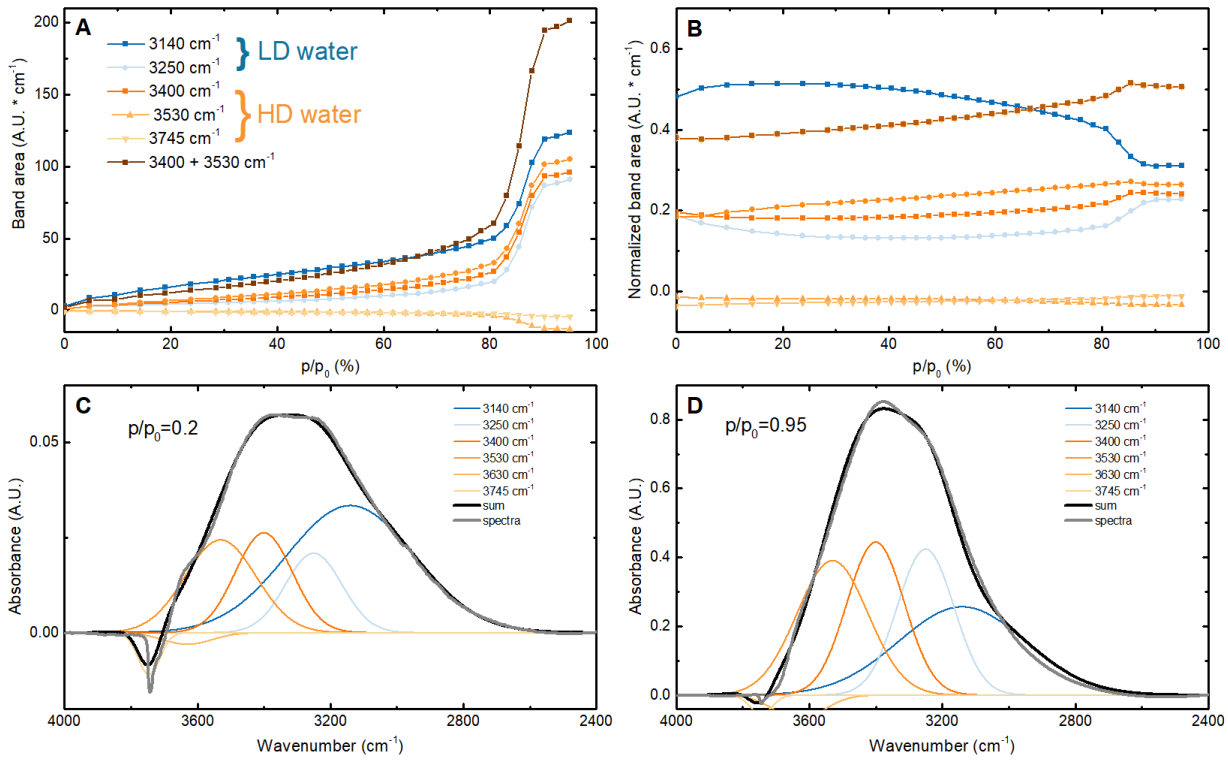

Figure 5: Deconvolution of ν(O-H) region obtained for F127 film during increasing p/p_0: peak area for different bands (A), band area normalized to the total band areas (B), multi-Gaussian fit of spectra before (C) and after (D) pore condensation.

All band areas except for the isolated silanol groups at 3745 cm^{-1} increase with p/p_0 (compare Figure 4A and 5A). As can be seen from Figure 4B and 5B, the relative amount of LD water changes significantly during pore condensation. Before pore condensation at p/p_0=0.5 or p/p_0=0.8, respectively, (see Figure 1B and 1C) the major fraction of water species corresponds to LD water. After pore condensation, the main fraction is the sum of peak III and IV that corresponds to HD, liquid-like water with low order.

If considering the simplest picture of pore filling, a complete layer of water on the materials surface is assumed before a subsequent layer is formed (compare Scheme 2A). Based on this hypothesis, several monolayers of water, most of which are strongly associated with the surface and hence contributing to the fraction of LD water, are forming before capillary condensation occurs. At this point, the remaining center part of the pores is filled predominately with bulk-like, less structured HD water. A stable concentration of the LD water after pore condensation would verify this hypothesis. However, our results do not fully agree with this simple picture, but show an increase of the LD water at and after capillary condensation at p/p_0= 0.5 and p/p_0=0.8 as visible in Figure 4A and 5A, respectively. From the abrupt increase of the LD fraction at capillary condensation we can assume that the center of the pore is not exclusively filled with HD water but also LD water. In return, the HD fraction is also growing less strongly from p/p_0= 0 on.

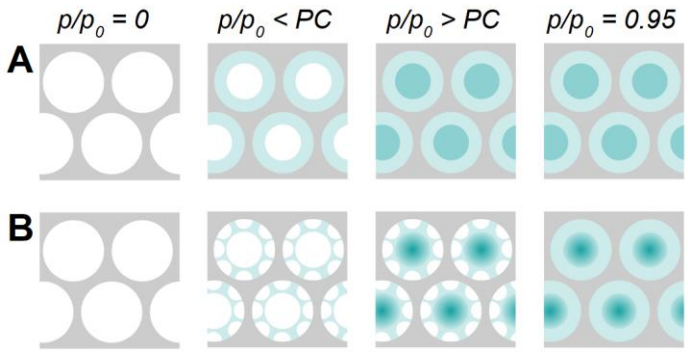

Scheme 2: Schematic representation of different hypothesis of water adsorption in mesopores for LD water (light blue) and HD water (dark blue) adsorption at different p/p_0. (A) Before pore condensation (PC) LD water fully convers the pore surface. (B) Pore surface is fully covered after pore condensation.

Kocherbitov *et al*. found a similar adsorption behavior and concluded that in contrast to the simple hypothesis, the pore surface is only partially covered with water and hydrophobic patches at the pore walls, *i.e.* spots with low silanol density, are wetted at higher relative vapor pressures after capillary condensation (compare Scheme 2B).[32,33] This conclusion is in accordance with our findings: The concentration of surface-associated water species, *i.e.* water, still increases after capillary condensation (Figure 4A and 5A).

Furthermore, the obtained water concentrations can be used to estimate the thickness of the LD water film with a monolayer thickness of 0.28 nm[48] in the fully filled pores (see ESI for calculation). Only at high humidity (p/p_0=0.95) the pores are fully filled and monolayers of water are not disrupted by hydrophobic patches (compare Scheme 2B). Therefore this analysis was only performed for the fully filled pores. For the calculations, we assumed a porous volume comprised of spheroids with pore diameter of b = 4.7 nm and a = 6.3 nm for the 3D hexagonal film, and b = 12.5 nm and a = 19.5 nm for the F127 film, respectively, with a retrieved from the anisotropy factor $q = a/b$ (see Table 1 in ESI). If assuming a monodisperse system, the calculations yield 3 and 7 monolayers for the CTAB and F127 film, respectively. These values represent an upper limit for the numbers of LD monolayers because pore interconnections and microporosity were excluded which leads to an underestimation of the pore surface. Even for this upper limit assumption, the number of monolayers for the CTAB film is smaller than the number of 4 monolayers reported for planar SiO_2.[49] However, PSD confirms pore interconnections > 2 nm for the F127 film and the microporosity of both films can be assessed from isotherms (see ESI) to be 8 % and 4 % of the total porosity for the CTAB and the F127 film, respectively. To account for the microporosity, we assumed a bidisperse system with pore diameters as given above and 1 nm micropores constituting 8 % and 4 %, respectively, of the total pore volume. This assumption may be not correct but is given as an example. This yielded 2 and 4 monolayers for the CTAB and F127 film, respectively. The result for the large pore system (F127 film) is in agreement with the previously reported number of 4 surface-induced ordered monolayers found on planer SiO_2.[49] However, the number of LD water monolayers found in the small pore film is considerably smaller.

For the CTAB 3D hexagonal film 3 and 2 monolayers of LD water with and without microporosity, respectively, were observed. These values agree well with the generally observed number of two surface-affected monolayers in confined fluids at pore surfaces.[50]
Note that the thicknesses of surface-induced structured water does not allow for conclusions about the overall water thickness *t* as needed for PSD calculations in the previous section.

CONCLUSION

In conclusion, we observed the evolution of water's structure in mesoporous silica films *in situ* during adsorption and desorption. In addition to the structural study of adsorbed water, ATR-FTIR spectroscopy is also used for determining the porosity and pore size distribution of the mesoporous silica films under study. The porosity and pore size distribution retrieved using the Kelvin equation are in excellent agreement with values obtained from established ellipsometric porosimetry. The high sensitivity of the stretching vibrations to the water molecule's states of hydrogen bonding enabled distinguishing bulk liquid and surface-induced ordered water, depending on its proximity to the surface. The IR spectra between 3000 and 3800 cm^{-1} were deconvolved giving the humidity-dependent development of different water species in SiO_2 mesopores. Based on this, the number of surface-induced ordered water monolayers was estimated and pores with a diameter of ca. 13 nm yielded values that coincide with reported values for water on planar SiO_2 surfaces, while smaller pores showed a significantly lower number of ordered water layers. Given these results, a drastic change in the water structure in confined spaces between a 5 and 13 nm pore diameter is observed.

In conclusion, we presented an instrumentally straightforward approach to study a variety of adsorption processes and phenomena in porous films *in situ* based on mid-IR ATR spectroscopy. Besides its application to porosimetry and analysis of adsorbed water's intermolecular structure, this method could be used for other adsorbates in porous materials and especially mixtures thereof to study displacement of one adsorbate by another based on characteristic IR bands. The presented setup allows for studying fundamental surface-molecule interactions beyond water as the absorption bands of many functional groups change upon adsorption depending on the adsorption mechanism.

ASSOCIATED CONTENT

Supporting Information.
The following files are available free of charge.

Characterization of mesoporous silica, calculation of pore anisotropy, determination of $d_{e,film}$ and corresponding refractive indices, determination of LD water monolayers (PDF)

AUTHOR INFORMATION

Corresponding Author

*bernhard.lendl@tuwien.ac.at

Funding Sources

This work is part of the AQUARIUS project, which has received funding from the European Union's Horizon 2020 research and innovation program under grant agreement No. 731465. This project is an initiative of the Photonics Public Private Partnership. J.H. acknowledges funding from the Competence Centre ASSIC – Austrian Smart Systems Research Center – within the COMET – Competence Centers for Excellent Technologies program. B.B. acknowledges funding from the Christiana Hörbiger fellowship.

ACKNOWLEDGMENT

X-ray diffraction was performed at the interfaculty X-Ray Center of TU Vienna. The authors thank IMEC/University of Ghent for providing cleaved Ge wafer samples.

REFERENCES

1. Brunel, D., Blanc, A. C., Galarneau, A. & Fajula, F. New Trends in the Design of Supported Catalysts on Mesoporous Silicas and their Applications in Fine Chemicals. in *Catalysis Today* **73,** 139–152 (Elsevier, 2002).
2. Clark, J. H., Macquarrie, D. J. & Tavener, S. J. The Application of Modified Mesoporous Silicas in Liquid Phase Catalysis. *Dalt. Trans.* **0,** 4297 (2006).
3. Macquarrie, D. J. Organically Modified Micelle Templated Silicas in Green Chemistry. *Topics in Catalysis* **52,** 1640–1650 (2009).
4. Walcarius, A. & Collinson, M. M. Analytical Chemistry with Silica Sol-Gels: Traditional Routes to New Materials for Chemical Analysis. *Annu. Rev. Anal. Chem.* **2,** 121–143 (2009).
5. Walcarius, A., Mandler, D., Cox, J. A., Collinson, M. & Lev, O. Exciting new directions in the intersection of functionalized sol–gel materials with electrochemistry. *J. Mater. Chem.* **15,** 3663 (2005).
6. Melde, B. J., Johnson, B. J. & Charles, P. T. Mesoporous Silicate Materials in Sensing. *Sensors* **8,** 5202–5228 (2008).
7. Wang, J. *et al.* New insights into the structure-performance relationships of mesoporous materials in analytical science. *Chemical Society Reviews* **47,** 8766–8803 (2018).
8. Verdaguer, A., Sacha, G. M., Bluhm, H. & Salmeron, M. Molecular Structure of Water at Interfaces: Wetting at the Nanometer Scale. *Chem. Rev.* **106,** 1478–1510 (2006).
9. Shimizu, T. K., Maier, S., Verdaguer, A., Velasco-Velez, J. J. & Salmeron, M. Water at surfaces and interfaces: From molecules to ice and bulk liquid. *Progress in Surface Science* **93,** 87–107 (2018).
10. Thiel, P. A. & Madey, T. E. The interaction of water with solid surfaces: Fundamental aspects. *Surface Science Reports* **7,** 211–385 (1987).
11. Ewing, G. E. Ambient Thin Film Water on Insulator Surfaces. *Chem. Rev.* **106,** 1511–1526 (2006).
12. Maréchal, Y. *et al.* FTIR study of condensed water structure. *J. Mol. Struct.* **111,** 146–155 (2007).

13. Verdaguer, A. *et al.* Growth and structure of water on SiO2films on Si investigated by kelvin probe microscopy and in situ X-ray spectroscopies. *Langmuir* **23,** 9699–9703 (2007).
14. Buck, U. & Huisken, F. Infrared spectroscopy of size-selected water and methanol clusters. *Chem. Rev.* **100,** 3863–3890 (2000).
15. Chen, L., He, X., Liu, H., Qian, L. & Kim, S. H. Water Adsorption on Hydrophilic and Hydrophobic Surfaces of Silicon. *J. Phys. Chem. C* **122,** 11385–11391 (2018).
16. Mallamace, F. *et al.* Evidence of the existence of the low-density liquid phase in supercooled, confined water. *Proc. Natl. Acad. Sci.* **104,** 424–428 (2007).
17. Soper, A. K. & Ricci, M. A. Structures of high-density and low-density water. *Phys. Rev. Lett.* **84,** 2881–2884 (2000).
18. Asay, D. B. & Kim, S. H. Evolution of the adsorbed water layer structure on silicon oxide at room temperature. *J. Phys. Chem. B* **109,** 16760–16763 (2005).
19. Asay, D. B., Barnette, A. L. & Kim, S. H. Effects of surface chemistry on structure and thermodynamics of water layers at solid-vapor interfaces. *J. Phys. Chem. C* **113,** 2128–2133 (2009).
20. Barnette, A. L. & Kim, S. H. Attenuated total reflectance infrared spectroscopy study of hysteresis of water and n-alcohol coadsorption on silicon oxide. *Langmuir* **28,** 15529–15536 (2012).
21. Boissiere, C. *et al.* Porosity and mechanical properties of mesoporous thin films assessed by environmental ellipsometric porosimetry. *Langmuir* **21,** 12362–12371 (2005).
22. Baklanov, M. R., Mogilnikov, K. P., Polovinkin, V. G. & Dultsev, F. N. Determination of pore size distribution in thin films by ellipsometric porosimetry. *J. Vac. Sci. Technol. B Microelectron. Nanom. Struct.* **18,** 1385 (2002).
23. Ricco, A. J., Frye, G. C. & Martin, S. J. Determination of BET surface areas of porous thin films using surface acoustic wave devices. *Langmuir* **5,** 273–276 (1989).
24. Tsionsky, V. & Gileadi, E. Use of the Quartz Crystal Microbalance for the Study of Adsorption from the Gas Phase. *Langmuir* **10,** 2830–2835 (1994).
25. Baumgartner, B., Hayden, J., Schwaighofer, A. & Lendl, B. In Situ IR Spectroscopy of Mesoporous Silica Films for Monitoring Adsorption Processes and Trace Analysis. *ACS Appl. Nano Mater.* **1,** 7083–7091 (2018).
26. Grosso, D. *et al.* Fundamentals of mesostructuring through evaporation-induced self-assembly. *Adv. Funct. Mater.* **14,** 309–322 (2004).
27. Karabudak, E. *et al.* Disposable Attenuated Total Reflection-Infrared Crystals from Silicon Wafer: A Versatile Approach to Surface Infrared Spectroscopy. *Anal. Chem.* **85,** 33–38 (2013).
28. Neimark, A. V. *et al.* Physisorption of gases, with special reference to the evaluation of surface area and pore size distribution (IUPAC Technical Report). *Pure Appl. Chem.* **87,** (2015).
29. Horikawa, T., Do, D. D. & Nicholson, D. Capillary condensation of adsorbates in porous materials. *Advances in Colloid and Interface Science* **169,** 40–58 (2011).

30. Ramer, G. & Lendl, B. in *Encyclopedia of Analytical Chemistry* (John Wiley & Sons, Ltd, 2013).
31. Kischkat, J. *et al.* Mid-Infrared Optical Properties of Thin Films of Aluminum Oxide, Titanium Dioxide, Silicon Dioxide, Aluminum Nitride, and Silicon Nitride. *Appl. Opt.* **51,** 6789–6798 (2012).
32. Kocherbitov, V. & Alfredsson, V. Hydration of MCM-41 studied by sorption calorimetry. *J. Phys. Chem. C* **111,** 12906–12913 (2007).
33. Kocherbitov, V. Properties of Water Confined in an Amphiphilic Nanopore. *J. Phys. Chem. C* **112,** 16893–16897 (2008).
34. Hwang, J., Kataoka, S., Endo, A. & Daiguji, H. Adsorption and Desorption of Water in Two-Dimensional Hexagonal Mesoporous Silica with Different Pore Dimensions. *J. Phys. Chem. C* **119,** 26171–26182 (2015).
35. Dubreuil, O. *et al.* TiO2 mesoporous thin films studied by Atmospheric Ellipsometric Porosimetry: A case of contamination. *Microporous Mesoporous Mater.* **145,** 1–8 (2011).
36. Lu, H. M. & Jiang, Q. Size-dependent surface tension and Tolman's length of droplets. *Langmuir* **21,** 779–781 (2005).
37. Tolman, R. C. The effect of droplet size on surface tension. *J. Chem. Phys.* **17,** 333–337 (1949).
38. Groen, J. C., Peffer, L. A. A. & Pérez-Ramírez, J. Pore size determination in modified micro- and mesoporous materials. Pitfalls and limitations in gas adsorption data analysis. *Microporous Mesoporous Mater.* **60,** 1–17 (2003).
39. Verdaguer, A. *et al.* Growth and Structure of Water on SiO 2 Films on Si Investigated by Kelvin Probe Microscopy and in Situ X-ray Spectroscopies. *Langmuir* **23,** 9699–9703 (2007).
40. Barrett, E. P., Joyner, L. G. & Halenda, P. P. The Determination of Pore Volume and Area Distributions in Porous Substances. I. Computations from Nitrogen Isotherms. *J. Am. Chem. Soc.* **73,** 373–380 (1951).
41. Kruk, M., Jaroniec, M. & Sayari, A. Application of Large Pore MCM-41 Molecular Sieves To Improve Pore Size Analysis Using Nitrogen Adsorption Measurements. *Langmuir* **13,** 6267–6273 (2002).
42. Ravikovitch, P. I. & Neimark, A. V. Density functional theory of adsorption in spherical cavities and pore size characterization of templated nanoporous silicas with cubic and three-dimensional hexagonal structures. *Langmuir* **18,** 1550–1560 (2002).
43. Ravikovitch, P. I. & Neimark, A. V. Experimental confirmation of different mechanisms of evaporation from ink-bottle type pores: Equilibrium, pore blocking, and cavitation. *Langmuir* **18,** 9830–9837 (2002).
44. Davis, K. M. & Tomozawa, M. An infrared spectroscopic study of water-related species in silica glasses. *J. Non. Cryst. Solids* **201,** 177–198 (1996).
45. De Aragão, B. J. G. & Messaddeq, Y. Peak separation by derivative spectroscopy applied to FTIR analysis of hydrolized silica. *J. Braz. Chem. Soc.* **19,** 1582–1594 (2008).

46. Brubach, J. B., Mermet, A., Filabozzi, A., Gerschel, A. & Roy, P. Signatures of the hydrogen bonding in the infrared bands of water. *J. Chem. Phys.* **122,** (2005).
47. Dokter, A. M., Woutersen, S. & Bakker, H. J. Inhomogeneous dynamics in confined water nanodroplets. *Proc. Natl. Acad. Sci.* **103,** 15355–15358 (2006).
48. Israelachvili, J. N. *Intermolecular and surface forces*. (Academic Press, 2011).
49. Asay, D. B. & Kim, S. H. Evolution of the adsorbed water layer structure on silicon oxide at room temperature. *J. Phys. Chem. B* **109,** 16760–16763 (2005).
50. Coasne, B., Galarneau, A., Pellenq, R. J. M. & Di Renzo, F. Adsorption, intrusion and freezing in porous silica: The view from the nanoscale. *Chemical Society Reviews* **42,** 4141–4171 (2013).

TOC